Hindawi
Mathematical Problems in Engineering
Volume 2018, Article ID 2091695, 14 pages
https://doi.org/10.1155/2018/2091695

Research Article

A Novel Analytical Method to Calculate the Amounts of Free and Adsorbed Gas in Shale Gas Production

Qingyu Li,[1] Peichao Li,[2] Wei Pang,[3] Quanfu Bi,[4] Zonghe Du,[5] Xuebin Li,[5] and Detang Lu [1]

[1]*Department of Modern Mechanics, University of Science and Technology of China, Hefei 230027, China*
[2]*School of Mechanical Engineering, Shanghai University of Engineering Science, Shanghai 201620, China*
[3]*Sinopec Research Institute of Petroleum Engineering, Beijing 100101, China*
[4]*Well Testing Company of CNPC Xibu Drilling Engineering Co., Ltd., Karamay 834000, China*
[5]*Exploration Division of Petro China Xinjiang Oilfield Branch Company, Karamay 834000, China*

Correspondence should be addressed to Detang Lu; dtlu@ustc.edu.cn

Received 14 March 2018; Accepted 23 May 2018; Published 20 June 2018

Academic Editor: Francisco J. Montáns

Shale gas has now become an important part of unconventional hydrocarbon resources all around the world. The typical properties of shale gas are that both adsorbed gas and free gas play important roles in gas production. Thus the contributions of free and adsorbed gas to the shale gas production have become a hot, significant, and challenging problem in petroleum engineering. This paper presents a new analytical method to calculate the amounts of free and adsorbed gas in the process of shale gas extraction. First, the expressions of the amounts of adsorbed gas, matrix free gas, and fracture free gas in shale versus the producing time are presented on the basis of Langmuir adsorption model and formation pressure distribution. Next, the mathematical model of multifractured horizontal wells in shale gas reservoirs is established and solved by use of Laplace transform and inversion to obtain the normalized formation pressure distribution. Finally, field case studies of two multifractured horizontal shale gas wells in China are carried out with the presented quantitative method. The amounts of adsorbed and free gas in production are calculated, and the adsorbed-to-total ratio is provided. The results show that the proposed method is reliable and efficient.

1. Introduction

In recent years, shale gas reservoirs have become a major natural gas resource [1]. Shale gas is expected to account for 30% of worldwide natural gas production by 2040 [2]. Besides free gas, a considerable amount of produced gas comes from desorption in shale gas reservoirs, which is different from the conventional gas reservoirs [3]. So the study of shale gas production behavior is of great significance in petroleum engineering. Many researchers have studied the distinct gas storage mechanisms in shale. Wang and Reed investigated the effects of organic matter on petrophysical properties, pore networks, and fluid flow in gas-shale systems and presented four types of porous media in productive gas-shale systems [4]. Zhang et al. presented that adsorbed gas in shale is mainly adsorbed in the organic matter and clay minerals, and free gas is compressed in the inorganic pores and fractures [5]. Xia et al. developed a new model to analyze production performance considering the coupling of free and adsorbed gas and performed sensitivity analyses of key parameters [6].

In view of the unique gas storage mechanisms of shale, both adsorbed gas and free gas play important roles in shale gas production [7]. Mengal and Wattenbarger pointed out that most of the desorption does not take place until there is considerable depletion of free gas [8]. Therefore, estimating the amounts of free and adsorbed gas in shale gas production accurately is vital to describe the production behavior [9]. This can provide theoretical basis and technical support for predicting production performance, adjusting and optimizing the well production system (for example, nozzle changing, or shut-ins).

The material balance equation is commonly used to the estimate of gas reserves [10, 11]. For shale gas reservoirs, Ambrose et al. formulated a new gas-in-place equation accounting for the organic pore space taken up by the adsorbed phase [12]. Orozco and Aguilera introduced a new

material balance equation considering the contributions of free, adsorbed, and dissolved gas [13]. Meanwhile, the free-to-adsorbed gas ratio in shale can be obtained by experiments. Liu et al. established an equation to estimate the ratio of free gas and adsorbed gas based on isotopic geochemical experimental data [14]. Liu and Sun presented an empirical formula to describe the relationship between the free-to-adsorbed ratio, porosity and acoustic amplitude attenuation coefficient [15]. With the above methods, the free and adsorbed gas reserves can be calculated. However, these methods are difficult to estimate the relations of adsorbed and free gas amounts in the formation versus producing time during shale gas production.

To the best of our knowledge, the approach to determine the transient proportion of free and desorbed gas during the production of shale gas wells has not been reported previously in the literature. Therefore, the objective of this study is to present a new quantitative method to estimate the dynamic contributions of free and adsorbed gas in shale gas production in the case of a multifractured horizontal well.

2. Calculation of Adsorbed and Free Gas in Shale

According to the mechanisms for gas storage and the typical pore structure of shale [16], we assume that the shale gas is stored as adsorbed gas and free gas in this work. Compared to the adsorbed and free gas, the quantities of dissolved gas in the formation are relatively minor; thus the dissolved gas is not considered in this work. The shale formation is assumed to be homogeneous, isotropic, and fully closed with rectangular boundaries.

In shale gas reservoirs, adsorbed gas accounts for about 20-85% of total gas [17]. Langmuir adsorption model [18] is usually employed to describe the gas adsorption in shale:

$$V_{ad} = \frac{V_L p}{p + p_L} \tag{1}$$

where V_L is Langmuir volume; p_L is Langmuir pressure; p is gas pressure; V_{ad} is adsorbed gas amount per unit mass of shale. p_L and V_L are indispensable parameters to describe the adsorption, which can be obtained by isothermal adsorption experiments[19–21].

As for shale gas reservoirs, multifractured horizontal wells are the most popular stimulation technique [22–24]. This leads to the fact that the free gas in the shale formation can be divided into two parts: matrix free gas and fracture free gas. Pan and Connell provided the expression of matrix free gas, which is shown as follows [25]:

$$V_m = \frac{\rho_{gm}}{\rho_{gsc}} \left(V_{pm} \left(1 - \mathrm{S}_{wm}\right) - \frac{V_{ad} \rho_{gsc}}{\rho_{ad}} \right) \tag{2}$$

where V_m is the amount of free gas in matrix per unit mass of shale, ρ_{gm} is gas density in the matrix, ρ_{gsc} is the gas density at standard condition, and V_{pm} is the effective matrix pore volume per unit mass of shale, which can be obtained by the effective porosity ϕ and the density of shale matrix ρ_m. S_{wm} is water saturation in the matrix and ρ_{ad} is the adsorbed phase density [26]. Many scholars have investigated the adsorbed phase density in shale through experiments. Considering our field cases are from the Jiaoshiba area, we take the adsorbed phase density as 0.373 g/cm^3, which is provided by Hu et al. [27] in the experiment study of Wufeng-Longmaxi shale in the Jiaoshiba area. The effective porosity of matrix ϕ is the key parameter to calculate the free gas in matrix and can be measured by experiments [28]. Considering the ultra-low porosity, methods such as image analysis [29] and water immersion porosimetry [30] can be used for estimating the porosity of shale.

The amount of fracture free gas can be described as

$$V_f = \frac{\rho_{gf}}{\rho_{gsc}} \left(V_{pf} \left(1 - S_{wf}\right) \right) \tag{3}$$

where V_f is the amount of free gas in fracture(s) per unit mass of shale; ρ_{gf} is gas density in the fracture(s); V_{pf} is fracture volume per unit mass of shale; and S_{wf} is water saturation in the fracture(s).

According to (1)-(3), we assume that the pressure distribution in the formation $p(x, y, t)$ is known, then the amounts of adsorbed gas in the formation Q_{ad} can be expressed as

$$Q_{ad}\left(\mathrm{t}\right) = \int_0^{x_e} \int_0^{y_e} \frac{V_L p\left(\mathrm{x}, \mathrm{y}, \mathrm{t}\right)}{p_L + p\left(\mathrm{x}, \mathrm{y}, \mathrm{t}\right)} dxdy \cdot h \left(1 - \phi_{ini}\right) \rho_m \tag{4}$$

where ρ_m is the density of shale matrix, ϕ is the porosity of the matrix, and x_e and y_e are the boundary lengths of the formation. The subscript *ini* represents the initial condition.

Substituting (4) into (2), we have the amounts of matrix free gas in the formation Q_m as follows:

$$\begin{aligned} Q_m\left(\mathrm{t}\right) = \int_0^{x_e} \int_0^{y_e} & \frac{p\left(\mathrm{x}, \mathrm{y}, \mathrm{t}\right) T_{sc}}{p_{sc} T z\left(p\right)} \left[\phi\left(p\right) \left(1 - \mathrm{S}_{wm}\right) \right. \\ & \left. - \frac{\rho_{gsc}}{\rho_{ad}} \frac{V_L p\left(\mathrm{x}, \mathrm{y}, \mathrm{t}\right)}{p_L + p\left(\mathrm{x}, \mathrm{y}, \mathrm{t}\right)} \left(1 - \phi_{ini}\right) \rho_m \right] dxdy \\ & \cdot h \end{aligned} \tag{5}$$

where T is the temperature. The subscript *sc* represents the standard condition, p_{sc} is 101325Pa, and T_{sc} is 298.15K. It is noted that $\phi(p)$ can be obtained by (13).

To estimate the amounts of fracture free gas, we make the following assumptions: (1) the pressure of each fracture is equal to the bottom-hole pressure; (2) the proppants to sustain the opening of the fractures are ignored; (3) the shape of fractures is cuboid.

Then (3) can be rewritten as

$$Q_f\left(\mathrm{t}\right) = \frac{p_{wf}\left(\mathrm{t}\right) T_{sc}}{p_{sc} T z\left(p_{wf}\right)} \left[2 \sum_{i=1}^{n} \mathrm{x}_{fi} \mathrm{wh} \left(1 - \mathrm{S}_{wf}\right) \right] \tag{6}$$

where Q_f is the amounts of fracture free gas in the formation, x_f denotes the fracture half-length, and p_{wf} is the bottom-hole pressure, and w is the width of fractures.

Note that the amounts of fracture free gas obtained by (6) are estimated values. We used (6) to estimate the order

of magnitude. In **Section 5.1** (**Case 1**), the amounts of matrix free gas and adsorbed gas are on the order of 10^8-10^9, while that of the fracture free gas is on the order of 10^5. Thus the fracture free gas can be **ignored** since it is much smaller as compared with matrix free gas and adsorbed gas. Moreover, we assume that the fractures have infinite conductivity in the following derivation, and the fractures can be regarded as a part of the wellbore. In this way, the fracture free gas should be considered in the wellbore storage.

The amounts of free and adsorbed gas in the formation of the n^{th} and $(n\text{-}1)^{th}$ day can be calculated by (4)-(6). Then the flow-rates of free and adsorbed gas in production at the n^{th} day equal the difference between the gas amounts in the formation of the n^{th} and $(n\text{-}1)^{th}$ day. That is,

$$q_{ad}(\mathrm{n}) = \left[Q_{ad}(\mathrm{n}-1) - Q_{ad}(\mathrm{n})\right]/1\,(day) \tag{7}$$

$$q_{free}(\mathrm{n}) = \left[Q_{m}(\mathrm{n}-1) - Q_{m}(\mathrm{n})\right]/1\,(day) \tag{8}$$

where q_{ad} represents the flow-rates of adsorbed gas and q_{free} is the flow-rates of free gas.

The adsorbed-to-total ratio R_{ad} in production, which denotes the flow-rates of adsorbed gas to total gas ratio, can be expressed as

$$R_{ad}(\mathrm{n}) = \frac{q_{ad}(\mathrm{n})}{q_{ad}(\mathrm{n}) + q_{free}(\mathrm{n})} \tag{9}$$

where n represents the n^{th} day.

3. Calculation of Pressure Distribution

As demonstrated in Section 2, we provide (4)-(9) to express the free and adsorbed gas amounts and flow-rates in shale gas production. We can see that it is of great importance to obtain the pressure distribution in the formation. As for shale gas reservoirs, multifractured horizontal wells technique is extensively employed to improve the productivity, especially in China. In this study, we consider that there is a horizontal well with multifractures in a fully closed rectangular formation, as shown in Figure 1.

In this section, the mathematical model of a multifractured horizontal well in the formation is first established, and then the pressure distribution is calculated by Laplace transform and inversion.

3.1. Assumptions. To establish the mathematical model for horizontal wells with multiple fractures in shale gas reservoirs, the following assumptions are made: (1) the reservoir has a uniform initial pressure and constant temperature; (2) the horizontal well is located in center of the formation. Along with the wellbore, multiple fractures are evenly distributed; (3) the properties of individual fractures are the same and the fractures are assumed to have infinite conductivity; (4) the fracture height is the same as net pay; (5) the horizontal well is cased or contributes little when compared with fractures; (6) the permeability and porosity varying with the pressure [31] and effects of gravity forces are negligible.

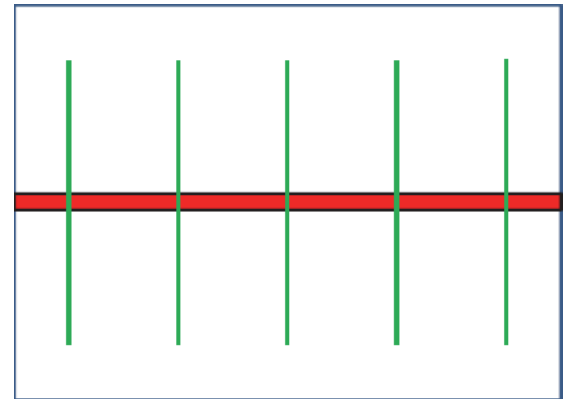

Figure 1: Schematic of a multifractured horizontal well in a fully closed rectangular formation.

3.2. Governing Equations. Under the above assumptions and conditions, we can write the governing equations as follows.

Flow Equation. For shale gas reservoirs, the continuity equation [32] is

$$\frac{\partial(\rho\phi)}{\partial t} + \nabla\cdot\left(\rho\frac{k}{\mu}\nabla p\right) = \frac{\partial V}{\partial t}B_g\rho \tag{10}$$

Then the flow equation of shale gas is

$$\frac{\partial}{\partial x}\left(\frac{kp}{\mu z}\frac{\partial p}{\partial x}\right) + \frac{\partial}{\partial y}\left(\frac{kp}{\mu z}\frac{\partial p}{\partial y}\right) = \frac{\partial}{\partial t}\left(\frac{\phi p}{z}\right) + \frac{p_{sc}T}{T_{sc}}\frac{\partial V}{\partial t} \tag{11}$$

where V is the concentration of gas, μ is the gas viscosity, z denotes the gas compressibility factor, t is the time, and k is the permeability.

Porosity and Permeability Equations. In this work, the permeability and the effective porosity vary with the pressure, and the relations are investigated by many scholars [33–36]. Raghavan and Chin presented the following relations, which is one of the most common relationships for shales [36]:

$$\frac{k}{k_{ini}} = \exp\left[-\gamma\left(p_{ini} - p\right)\right] \tag{12}$$

$$\frac{\phi}{\phi_{ini}} = \exp\left[-\beta\left(p_{ini} - p\right)\right] \tag{13}$$

where β and γ are material constants and can be measured by experiments.

Gas Diffusion Equation. The equation of gas concentration is given as follows [37]:

$$\frac{\partial V}{\partial t} = \frac{6D\pi^2}{R^2}\left(V_E - V\right) \tag{14}$$

where D is the gas diffusion coefficient; R is the outer radius in gas diffusion; V_E is the equilibrium volumetric gas concentration.

The adsorption equation of shale gas can be expressed by Langmuir adsorption model, then we can obtain

$$V_E = \frac{V_L p}{p_L + p}, \qquad V_{ini} = \frac{V_L p_{ini}}{p_L + p_{ini}} \tag{15}$$

where V_L is Langmuir volume and p_L is Langmuir pressure.

Outer Boundary Condition. The outer boundary condition can be expressed by

$$\left.\frac{\partial p(x,y)}{\partial x}\right|_{y=y_e} = 0 \tag{16}$$

$$\left.\frac{\partial p(x,y)}{\partial y}\right|_{x=x_e} = 0 \tag{17}$$

where x_e and y_e represent the boundary of the formation.

Inner Boundary Condition. According to the definition of wellbore storage and skin effects [38], the inner boundary conditions are

$$p_{wf}(t) = p_w(t) - \frac{q(t)B\mu}{2\pi kh} S_{kin} \tag{18}$$

$$C\frac{dp_{wf}}{dt} + q(t) = \sum_{j=1}^{n} q_j \tag{19}$$

where p_{wf} is the bottom-bole pressure considering the skin effects while p_w is the bottom-hole pressure of the open hole well. q is the measured wellhead flow-rate; h is the formation thickness; B is the volume factor; q_j means the flow-rate of fracture j, while q stands for the sum. C is the wellbore storage constant and S_{kin} is the skin factor.

The Dimensionless Equations. Incorporating the pressure-sensitive effect and PVT characteristics of shale gas and solid matrix, the normalized pressure and normalized time can be defined [39] as

$$m = \frac{1-\phi_{ini}}{k_{ini}} \frac{\mu_{gini} z_{ini}}{p_{ini}} \int \frac{p}{\mu_g(p) z(p)} \left[\frac{k(p)}{1-\phi(p)}\right] dp \tag{20}$$

$$t_a = \left(\frac{\phi \mu_g c_g}{kq}\right)_{ini} \int_0^t \frac{k(p) q(\tau) d\tau}{\phi(p) \mu_g(p) c_g(p)} = \left(\frac{\phi \mu_g c_g}{kq}\right)_{ini} \int_0^t \frac{k(p) dp}{\phi(p) \mu_g(p) c_g(p)} \cdot \frac{q(\tau)}{dp/d\tau} \tag{21}$$

The dimensionless normalized pressure and dimensionless normalized time are

$$m_D = \frac{2\pi k_{ini} h [m_{ini} - m(t_a)]}{B_{gini} \mu_{ini} q(t_a)} \tag{22}$$

$$t_D = \frac{k_{ini} t_a}{\alpha L^2} \tag{23}$$

where c_g is the gas compressibility; $L = \sum_{i=1}^{n} x_{fi}$ is the sum of fracture half-lengths, with x_{fi} being the half-length of fracture i and n being the number of fractures. $\alpha = \phi \mu c g + k_i h p_{sc} T z_i / q_{sc} B_{gi} T_{sc} p_i$ is the comprehensive storage coefficient. The subscript g represents the gas.

According to (20)-(23), the following quantities are defined: the storage ratio $\omega = \phi_{ini} \mu_{ini} C_{gini} / \alpha$; the interporosity flow coefficient $\lambda = \alpha L^2 / k_{ini} \tau$; the dimensionless coordinates $x_D = x/L$, $y_D = y/L$, $x_{eD} = x_e/L$, and $y_{eD} = y_e/L$; the adsorption time $\tau = R^2/6\pi^2 D$.

Here we define $V_D = V_{ini} - V$, $V_{ED} = V_{ini} - V_E$, where V_{ini} is the gas concentration at the initial time ($t = 0$).

With the above definitions, (11)-(14) can be rewritten in dimensionless forms:

$$\frac{\partial^2 m_D}{\partial x_D^2} + \frac{\partial^2 m_D}{\partial y_D^2} = \omega \frac{\partial m_D}{\partial t_D} - (1-\omega) \frac{\partial V_D}{\partial t_D} \tag{24}$$

$$\frac{\partial V_D}{\partial t_D} = \frac{1}{\lambda} (V_{ED} - V_D) \tag{25}$$

Herein,

$$V_{ED} = V_E - V_{ini} = \frac{V_L p_L (p - p_{ini})}{(p_L + p)(p_L + p_{ini})} = \frac{V_L m_L (m - m_{ini})}{(m_L + m)(m_L + m_i)} = -\gamma m_D \tag{26}$$

$$\gamma = -\frac{q B_{gini} \mu_{ini}}{2\pi k_{ini} h} \frac{V_L m_L}{(m_L + m)(m_L + m_{ini})} \tag{27}$$

Here, γ can be considered as a constant within the common pressure range of interest and can be evaluated at $m = m_i$ [37]. Then (27) can be rewritten as

$$\gamma = \frac{q_{ini} B_{gini} \mu_{ini}}{2\pi k_{ini} h} \frac{V_L m_L}{(m_L + m_{ini})(m_L + m_{ini})} = \frac{q_{ini} B_{ini} \mu_{ini} V_L m_L}{4\pi k_{ini} h (m_L + m_{ini})} \tag{28}$$

where m_L and m_{ini} are the normalized pressure (obtained by using (20)) corresponding to p_L and p_{ini}.

Correspondingly, the boundary condition in dimensionless form is

$$m_{wfD} = m_{wD} + S_{kin} \tag{29}$$

$$C_D \frac{dm_{wfD}}{dt_D} + \sum q_{Dj} = 1 \tag{30}$$

$$\left.\frac{\partial p_D}{\partial x_D}\right|_{y_D = y_{eD}} = 0 \tag{31}$$

$$\left.\frac{\partial p_D}{\partial y_D}\right|_{x_D = x_{eD}} = 0 \tag{32}$$

where the dimensionless flow-rate q_{Dj}=q_j/q denotes the flow-rate contribution of the fracture j; $C_D = \mu_{ini} B_{gini} C / 2\pi\alpha h L^2$ is the dimensionless wellbore storage constant.

3.3. Solution Formulation

3.3.1. Laplace Transform. By implementing Laplace transform on (24)-(25), we obtain

$$\frac{\partial^2 \overline{m}_D}{\partial x_D^2} + \frac{\partial^2 \overline{m}_D}{\partial y_D^2} = \omega s \overline{m}_D - (1-\omega)\, s \overline{V}_D \tag{33}$$

$$s\overline{V}_D = \frac{1}{\lambda}\left(\overline{V}_{ED} - \overline{V}_D\right) \tag{34}$$

where s is the Laplace operator and the overbar "–" denotes Laplace transform.

With (33)-(34), the following equation is obtained:

$$\frac{\partial^2 \overline{m}_D}{\partial x_D^2} + \frac{\partial^2 \overline{m}_D}{\partial y_D^2} = f(s)\, \overline{m}_D \tag{35}$$

where $f(s) = [\omega + \gamma(1-\omega)/(s\lambda + 1)]s$.

3.3.2. Solutions in Laplace Domain. For a multifractured horizontal well in the rectangle formation, we solve (35) by Newman's method and Duhamel's principle.

Horne and Temeng presented a method based on Newman's principle [40] to calculate the bottom-hole pressure for multifractured horizontal wells [41]. Based on Horne and Temeng's method, we investigate a multifractured horizontal shale gas well in a fully closed rectangular formation ($x_e \times y_e$) using Duhamel's principle [42]. The flow-rate and normalized pressure in Laplace domain shall satisfy the following equations:

$$\sum_{j=1}^{n} \overline{q}_{Dj} = \frac{1}{s} \tag{36}$$

$$\overline{m}_{wDi}\left(f(s)\right) = \sum_{j=1}^{n} s\overline{q}_{Dj} \overline{m}_{Dij}\left(f(s)\right) \tag{37}$$

where

$$\overline{m}_{Dij}\left(f(s)\right) = \pi \int_0^{\infty} S_{xD}\left(\mathrm{x}_{wDi}, x_{wDj}, t_D\right) \cdot S_{yD}\left(\mathrm{y}_{wDi}, \mathrm{y}_{wDj}, t_D\right) e^{-f(s)t_D} dt_D \tag{38}$$

with

$$S_{xD} = \frac{2}{x_{eD}}\left[1 + \frac{2x_{eD}}{\pi}\sum_{n=1}^{\infty}\frac{1}{n}\exp\left(-\frac{n^2\pi^2 t_D}{x_{eD}^2}\right)\cdot \sin\frac{n\pi}{x_{eD}} \cdot \cos\frac{n\pi x_{wD\,j}}{x_{eD}} \cos\frac{n\pi x_{wD\,i}}{x_{eD}}\right] \tag{39}$$

$$S_{yD} = \frac{1}{y_{eD}}\left[1 + 2\sum_{n=1}^{\infty}\frac{1}{n}\exp\left(-\frac{n^2\pi^2 t_D}{y_{eD}^2}\right)\cos\frac{n\pi y_{wD\,j}}{y_{eD}} \cdot \cos\frac{n\pi y_{wD\,i}}{y_{eD}}\right] \tag{40}$$

where m_{Dij} is the normalized pressure at fracture i due to production at fracture j; x_{wDj} and y_{wDj} mean the location of fracture j; x_{eD} and y_{eD} are the boundaries of the formation.

Considering the wellbore storage and skin effects, with (29)-(30) we can rewrite (36)-(37) as

$$\sum_{j=1}^{n} \overline{q}_{Dj} = \frac{1}{s} - C_D s \overline{m}_{wfDi} \tag{41}$$

$$\overline{m}_{wfDi}\left(f(s)\right) = \sum_{j=1}^{n}\left[s\overline{q}_{Dj}\overline{m}_{Dij}\left(f(s)\right) + \overline{q}_{Dj}\cdot S_{kin}\right] \tag{42}$$

As all the fractures are connected by the horizontal well, the pressure of each fracture at the horizontal wellbore $\overline{m}_{wDi}$ can be regarded as the same. According to (41)-(42), the matrix equation can be established as

$$\begin{bmatrix} s\overline{m}_{D11}+\mathrm{S}_{kin} & s\overline{m}_{D12}+\mathrm{S}_{kin} & s\overline{m}_{D13}+\mathrm{S}_{kin} & \cdots & s\overline{m}_{D1n}+\mathrm{S}_{kin} & -1 \\ s\overline{m}_{D21}+\mathrm{S}_{kin} & s\overline{m}_{D22}+\mathrm{S}_{kin} & s\overline{m}_{D23}+\mathrm{S}_{kin} & \cdots & s\overline{m}_{D2n}+\mathrm{S}_{kin} & -1 \\ \cdots & & & & & \\ s\overline{m}_{Dk1}+\mathrm{S}_{kin} & s\overline{m}_{Dk2}+\mathrm{S}_{kin} & s\overline{m}_{Dk3}+\mathrm{S}_{kin} & \cdots & s\overline{m}_{Dkn}+\mathrm{S}_{kin} & -1 \\ \cdots & & & & & \\ s\overline{m}_{Dn1}+\mathrm{S}_{kin} & s\overline{m}_{Dn2}+\mathrm{S}_{kin} & s\overline{m}_{Dn3}+\mathrm{S}_{kin} & \cdots & s\overline{m}_{Dnn}+\mathrm{S}_{kin} & -1 \\ s & s & s & \cdots & s & 0 \end{bmatrix} \begin{bmatrix} \overline{q}_{D1} \\ \overline{q}_{D2} \\ \cdots \\ \overline{q}_{Dk} \\ \cdots \\ \overline{q}_{Dn} \\ \overline{m}_{wfD} \end{bmatrix} = \begin{bmatrix} 0 \\ 0 \\ \cdots \\ 0 \\ \cdots \\ 0 \\ 1 - C_D s^2 \overline{m}_{wfD} \end{bmatrix} \tag{43}$$

Clearly, $\overline{q}_{Dj}$ can be obtained by solving (43). Thus, the dimensionless normalized pressure distribution in Laplace domain is

$$\overline{m}_D\left(x_D, \mathrm{y}_D, f(s)\right) = \sum_{j=1}^{n} s\overline{q}_{Dj} \cdot \pi \cdot \int_0^{\infty} S_{xDj}\left(\mathrm{x}_D, \mathrm{x}_{wD\,j}, t_D\right) S_{yDj}\left(\mathrm{y}_D, y_{wD\,j}, t_D\right) \cdot e^{-f(s)t_D} dt_D \tag{44}$$

Table 1: Simulation parameters.

Parameters	Values (units)	Parameters	Values (units)
k	0.001 (md)	x_{f1}	60 (m)
C	1×10^{-6} (m^3/Pa)	x_{w1}	330 (m)
S_{kin}	0	x_{f2}	80 (m)
h	10 (m)	x_{w2}	370 (m)
ϕ	5%	x_{f3}	40 (m)
T	323.15 (K)	x_{w3}	420 (m)
V_L	7.5 (m^3/m^3)	x_{f4}	90 (m)
p_L	7.5 (MPa)	x_{w4}	480 (m)

where

$$S_{xDj} = \frac{2}{x_{eD}}\left[1 + \frac{2x_{eD}}{\pi}\sum_{n=1}^{\infty}\frac{1}{n}\exp\left(-\frac{n^2\pi^2 t_D}{x_{eD}^2}\right) \cdot \sin\frac{n\pi}{x_{eD}}\cos\frac{n\pi x_{wDj}}{x_{eD}}\cos\frac{n\pi x_D}{x_{eD}}\right] \tag{45}$$

$$S_{yDj} = \frac{1}{y_{eD}}\left[1 + 2\sum_{n=1}^{\infty}\frac{1}{n}\exp\left(-\frac{n^2\pi^2 t_D}{y_{eD}^2}\right)\cos\frac{n\pi y_{wDj}}{y_{eD}}\cos\frac{n\pi y_D}{y_{eD}}\right] \tag{46}$$

3.3.3. Solutions in Physical Domain. The bottom-hole normalized pressure as well as the flow-rate in each fracture in physical domain can be obtained by inverse Laplace transform. We apply Stehfest's method for inverse Laplace transform [43].

Equation (44) can be inverted by Stehfest's method as follows:

$$m_D(x_D, y_D, t_D) = \frac{\ln 2}{t}\sum_{i=1}^{N} V_i \overline{m}_D(x_D, y_D, f(s)) \tag{47}$$

where $V_i = (-1)^{N/2+i}\sum_{k=[(i+1)/2]}^{\min(i,N/2)}(k^{N/2+1}(2k)!/(N/2-k)!k!(k-1)!(i-k)!(2k-i)!)$.

Then the pressure distribution $p(x, y, t)$ can be obtained by (20)-(23) and (47). With (4)-(9), the amounts of free and adsorbed gas in the formation as well as flow-rates can be calculated and determined.

3.4. Model Validation. In this section, the model presented in this study is compared with a numerical simulator for shale gas reservoirs developed by Li et al. [44].

The reservoir size is 800 m × 800 m and the horizontal well is located in the center of the reservoir. The well is 200 m long with 4 symmetrical fractures and produces for 100 days at a constant flow-rate of 4000 m^3/d. The basic data are given in **Table 1**, and **Figure 2** shows the grids of the multifractured horizontal well.

The comparison of bottom-hole pressure in **Figure 3** shows that there is a perfect match between our model and the numerical simulator. The bottom-hole pressures at 2400 hours are 12.03771 MPa (the numerical simulator) and 12.04841 MPa (the proposed method), and the relative error is 0.09%. The results confirm the validity of the proposed method.

4. Implementing procedure

In summary, the overall implementing procedure for multifractured horizontal wells in shale gas reservoirs is given in the following.

Step 1. Verify the rock, fluid, and completion data such as viscosity, fluid compressibility, formation volume factor, porosity, and net pay, and obtain corresponding adsorbed quantity data from adsorption experiment.

Step 2. Based on the available field records and fluid property correlations, establish the mathematical model in shale gas reservoirs, and then the relation between dimensionless bottom-hole normalized pressure m_D and dimensionless normalized time t_D can be obtained analytically with (43), (44), and (47). See **Section 3** for details.

Step 3. According to (20)-(23) and measured history data, the $m_D \sim p$ and $t_D \sim t$ relations can be obtained, and the pressure distribution $p(x, y, t)$ in the shale formation can be calculated based on $m_D(x_D, y_D, t_D)$.

Step 4. By substituting $p(x, y, t)$ into (4)-(9), the time-dependent quantities and ratio of adsorbed and free gas in the shale formation during production can be obtained.

5. Field Examples

In this section, two filed cases of shale gas wells in China are studied with the presented method. The bottom-hole pressure and flow-rate history as well as basic parameters are offered first. Then the pressure distribution $p(x, y, t)$ is obtained with the method proposed in Section 3. The flow-rates of free and adsorbed gas in production verses time are plotted, and the adsorbed-to-total ratio is obtained.

5.1. Case 1. The case of a 24888-hour data of multifractured horizontal shale gas well in China is investigated. And the history of bottom-hole pressure and flow-rate is shown in

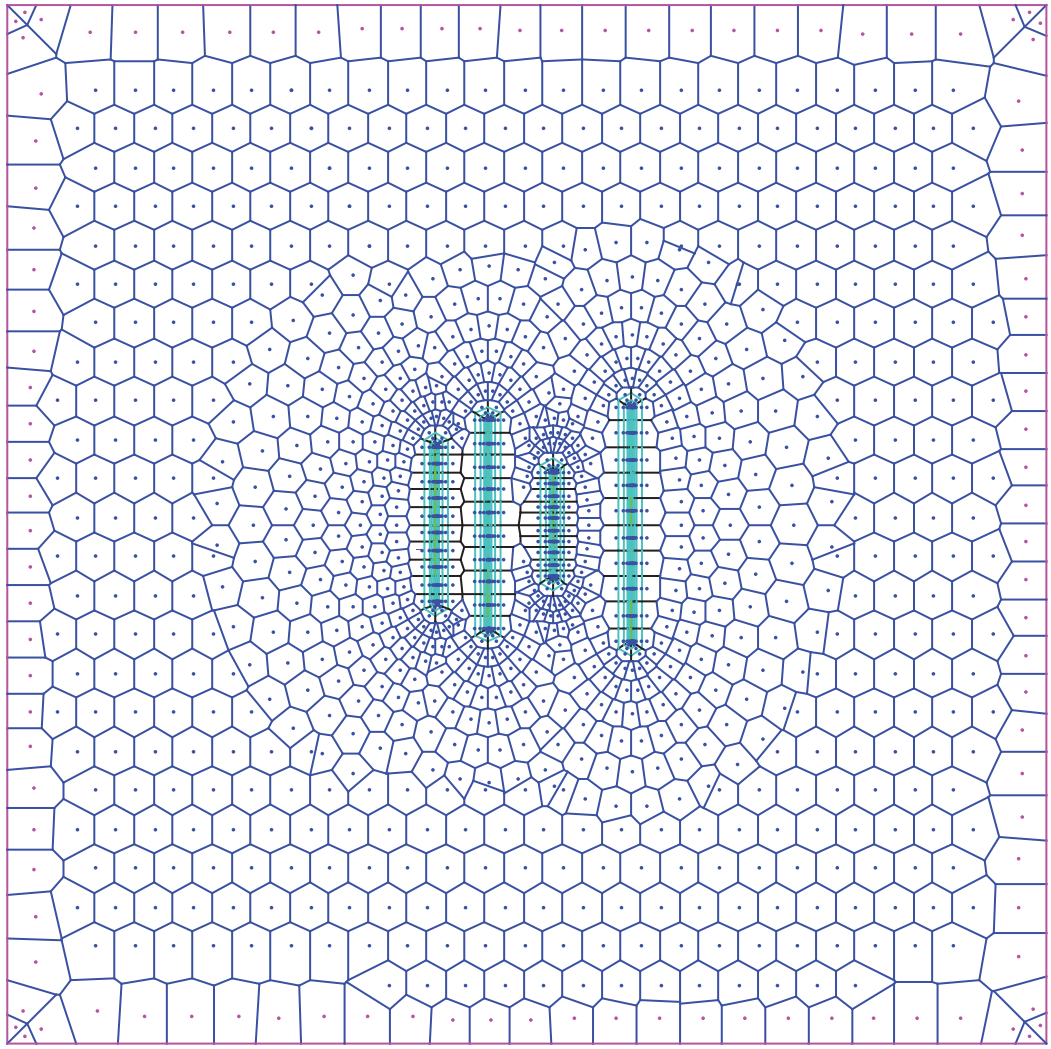

Figure 2: Multifractured horizontal well grids.

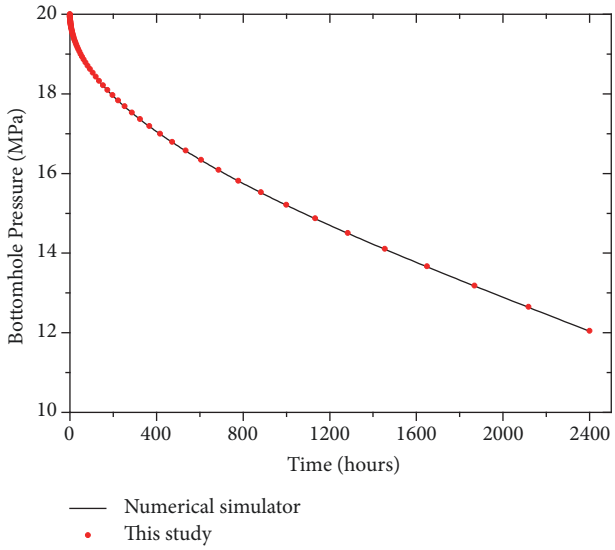

Figure 3: Bottom-hole pressure comparison.

Figure 4. From Figure 4, it can be seen that the flow-rate decreased in the first months and then kept stabilized while the pressure decreased most of the time.

The dimensions of the formation are estimated as 1200m×600m and the 1008-meter-long horizontal well with 7 fractures of equal length is located in the center of the formation. The basic parameters of the well are listed in Table 2.

With (20) and (47), the pressure distribution can be obtained. Figures 5 and 6 represent the pressure distribution in the shale gas formation at the 8016^{th} hour and the 17016^{th} hour respectively as examples. The computation time of this case is less than 0.1s.

Through (4)-(5), the amounts of free and adsorbed gas in the formation can be estimated. Figure 7 shows the relations of free and adsorbed gas amounts in the formation versus time. Clearly, the original free gas in place is about 3.0×10^8 (m^3), while the original adsorbed gas in place is about 1.3×10^8 (m^3). And we can see that the free gas decreases faster than

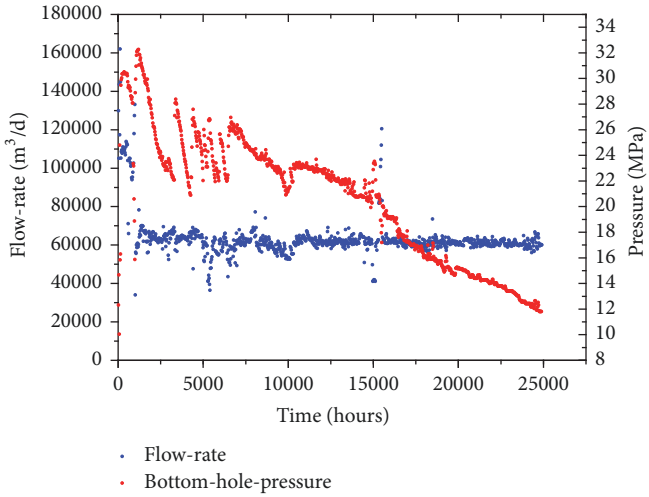

Figure 4: History of flow-rate and bottom-hole pressure for case 1.

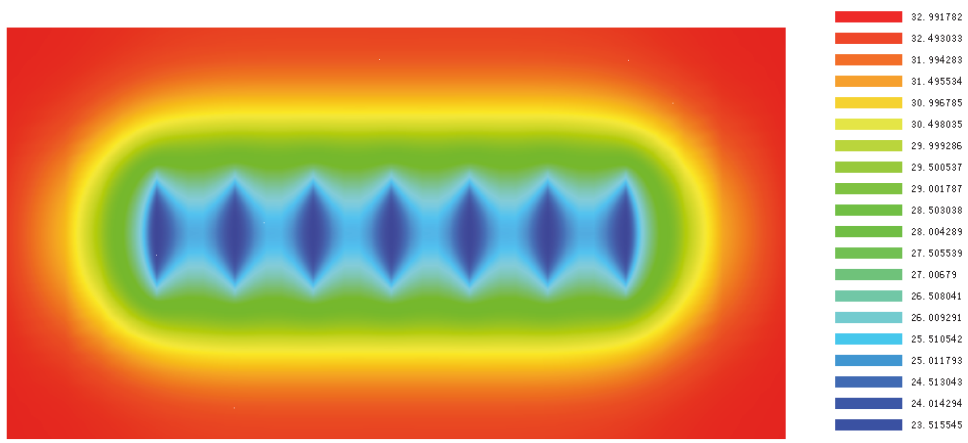

Figure 5: Contour of pressure at the 8016th hour.

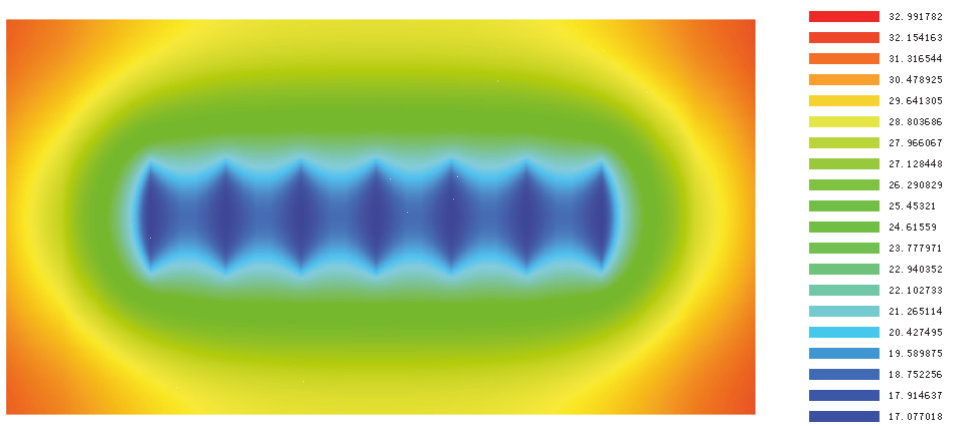

Figure 6: Contour of pressure at the 17016th hour.

Table 2: Parameters of the shale gas well in case 1.

Basic parameters	Values
Initial formation pressure	33(MPa)
Net pay thickness	38(m)
Temperature	80.96(°C)
Porosity	0.048
Material constant β	1.53×10^{-3}(MPa^{-1})
Material constant γ	0.043 (MPa^{-1})
Langmuir volume	2.98(m^3/t)
Langmuir pressure	6.02(MPa)
Shale density	2.61(t/m^3)
Water saturation	0.05
Fracture half-length	90(m)

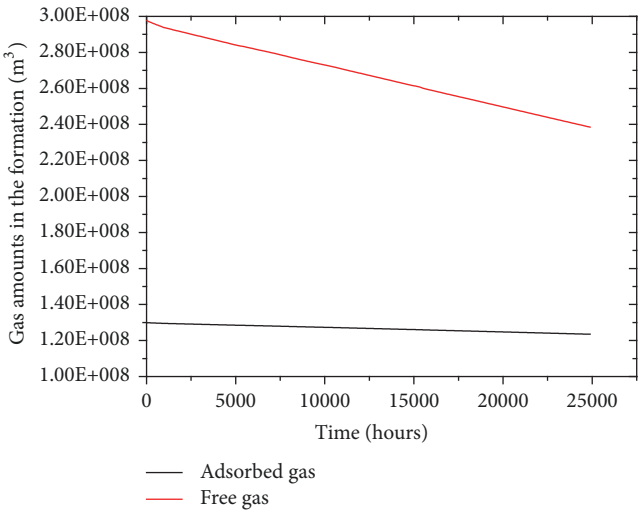

Figure 7: Amounts of adsorbed and free gas in the formation for case 1.

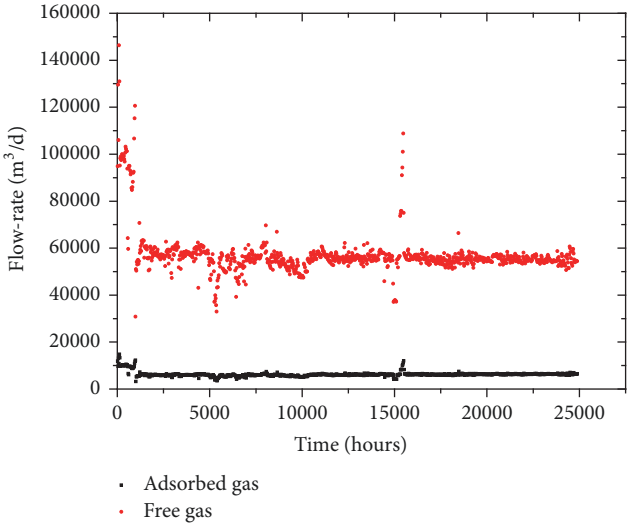

Figure 8: Flow-rates of adsorbed and free gas for case 1.

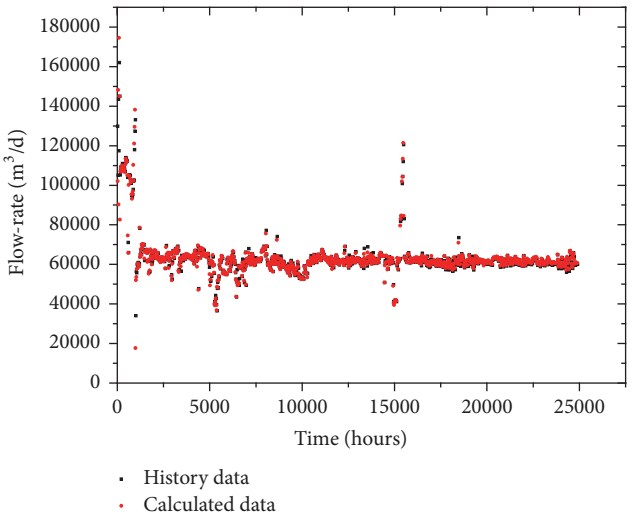

Figure 9: Comparison of calculated flow-rates and history data.

the adsorbed gas. The main reason should be that the bottom-hole pressure is relatively high, leading to the slow desorption process.

By use of Figure 7, the flow-rates of free and adsorbed gas in production can be calculated. Figure 8 shows the relations of free and adsorbed gas flow-rates versus time. It is clear that the flow-rate of adsorption gas is around 6000 m^3 /d while the flow-rate of free gas is approximate to 60000 m^3 /d. This is to say, the flow-rate of free gas is much bigger than the adsorbed gas in this case.

The sum of free and adsorbed gas, which is the total gas production estimated, is compared with the history data of gas flow-rate in Figure 9. We can see that the two lines are in good agreement, and the average error is less than 4%.

The adsorbed-to-total ratio R_{ad} in production, which means the flow-rates of adsorbed gas to total gas ratio is given in Figure 10. On the whole, the ratio is around 10% and increases with time slowly.

Note that the producing time of this case is not long enough, and the simulated adsorbed-to-total ratio in gas production is quite low. This can explain why the production decreased severely in the first 1000 hours. When the shale wells start to produce, the bottom-hole pressure is quite high. Most of free gas flows sluggishly in the matrix due to the low permeability, and the desorption cannot take place too much on account of the high pressure. Thus the production is manly contributed by the gas in the wellbore and fractures. With the free gas in and around fractures having flew into the wellbore and been exploited, the gas production decreases inevitably. It can be seen that the flow-rate kept stabilized since 1000th hour, the main reason should be that the flow-rate was not high, and the flow-rates of matrix free gas and adsorbed gas can satisfy the production.

Based on the above results, it can be predicted that the free gas will still make the main contribution to shale gas production in the following years. As time progresses, the formation pressure decreases gradually, and the ratio of adsorbed gas in production will increase accordingly.

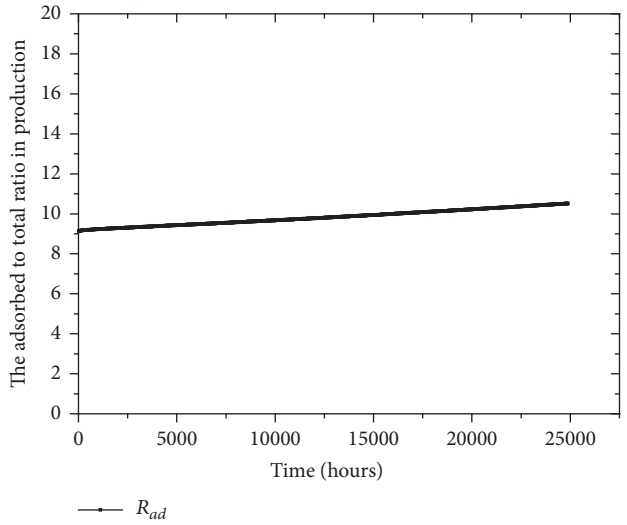

Figure 10: The adsorbed-to-total ratio R_{ad} in production.

5.2. Case 2. Another case of an 8448-hour data of multi-fractured horizontal shale gas well in China is investigated. The block of this well is different from the well in case 1. The history of bottom-hole pressure and flow-rate is shown in Figure 11. It can be seen that the flow-rate decreased in the most time. The pressure decreased quite rapidly in the first 2000 hours. The main reason may be that there is a considerable amount of liquid production in the early stage.

The 1500-meter-long horizontal well with 8 fractures of equal length is located in the center of the formation. The dimensions of the formation are estimated as 1700m×800m. The basic properties of the well are listed in Table 3. Compared with the well of case 1, the shale density is relatively high, and the porosity, Langmuir volume, and Langmuir pressure are a little higher.

Figures 12 and 13 represent the pressure distribution in the shale gas formation at the 1008th hour and the 3024th hour, respectively. As the flowing time is short, we can see that the flow concentrates around the fractures. The flow regime is transforming from fracture radial flow to formation linear flow.

Figure 14 shows the relations of free and adsorbed gas amounts in the formation versus producing time. It is seen that the original free gas in place is about 1.24×10^9 (m^3), while the original adsorbed gas in place is about 5.27×10^8 (m^3). The original gas in place of this well is bigger than the well of case 1.

By use of Figure 14, the flow-rates of free and adsorbed gas in production can be calculated. The relations of free and adsorbed gas flow-rates versus time are shown in Figure 15.

The calculated total gas flow-rate is compared with the history data of the well in Figure 16. It shows that the two lines are in good agreement, and the average error is about 6%. Compared with case 1, the quality of history matching is not so good. Probably the main reason is that the considerable liquid production in the early stage affects the calculation of pressure distribution in the formation.

Table 3: Parameters of the shale gas well in case 2.

Basic parameters	Values
Initial formation pressure	44(MPa)
Net pay thickness	46(m)
Temperature	79.6(°C)
Porosity	0.071
Material constant β	1.45×10^{-3}(MPa^{-1})
Material constant γ	0.032 (MPa^{-1})
Langmuir volume	4.0(m^3/t)
Langmuir pressure	8.62(MPa)
Shale density	2.713(t/m^3)
Water saturation	0.04
Fracture half-length	128(m)

The adsorbed-to-total ratio R_{ad} in production is given in Figure 17. The ratio increases with time, about 0.3% in one year. The obtained ratio of adsorbed gas in production is slightly higher than case 1.

Note that the producing time of case 2 are not long, and the simulated adsorbed-to-total ratio in gas production is about 11-12%. The main reason why the production decreased severely in this case is the same as case 1. The only difference is that the producing time is shorter and there is no data segment of stabilized flow-rate.

Based on the above results, it can be forecasted that the free gas will still contribute mainly to shale gas production in the following years. As time increases, the formation pressure decreases gradually, leading to the fact that the ratio of adsorbed gas in production will increase accordingly.

5.3. Discussion. There are still about 4% and 6% errors in history matching of gas production. Probably, the main reasons are as follows:

(1) The porosity, Langmuir volume, and Langmuir pressure are all obtained by experiments, and these values may not be accurate enough due to the nanoscaled pores in shale.

(2) Due to the hydraulic fracturing technique, there is commonly remaining fracturing liquid producing during gas production. This will lead to the decline of bottom-hole pressure and affect the pressure calculation.

In order to reduce the errors, improving the precisions of the experiments is an effective means. More reasonable mathematical models can be helpful as well. On the other hand, the two-phase (shale gas and fracturing liquid) flow equation can describe the flow in shale gas reservoirs more accurately during production. However, it is difficult to solve this equation in current analytical ways due to its complexity.

In this section, combining with the history data of two wells, we apply the proposed method to provide the relations of free and adsorbed gas amounts in the formation versus producing time. Then the verification is conducted by history matching of gas flow-rate. The adsorbed-to-total ratios in production of these two wells are about 10%, which agrees with the results reported by other scholars (e.g., see [25]).

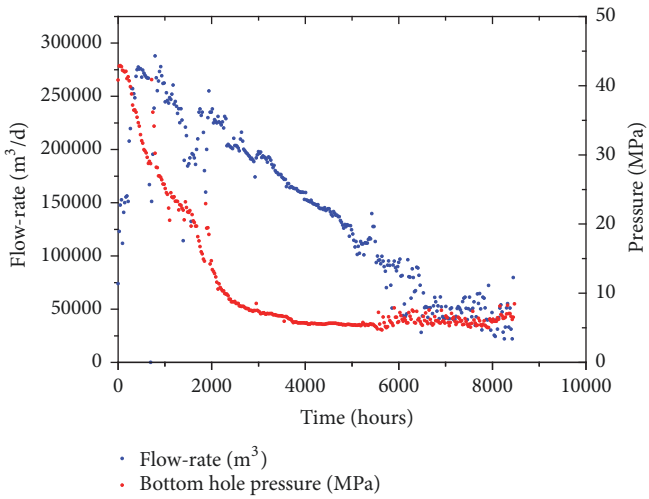

Figure 11: History of flow-rate and bottom-hole pressure for case 2.

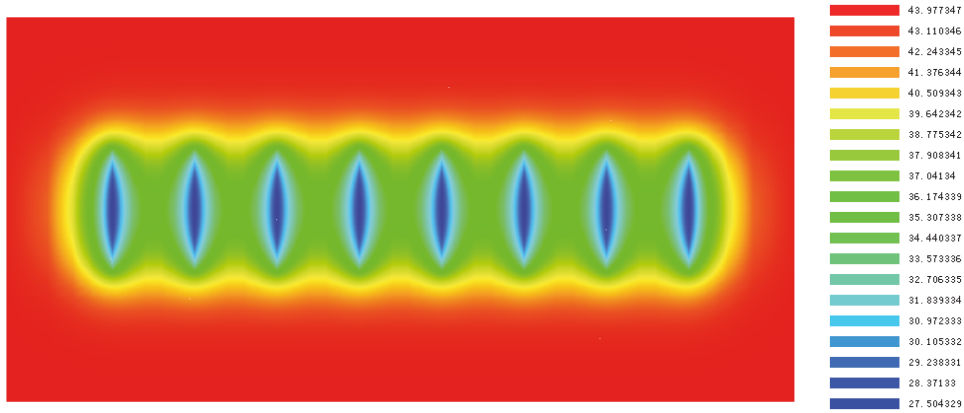

Figure 12: Contour of pressure at the 1008th hour.

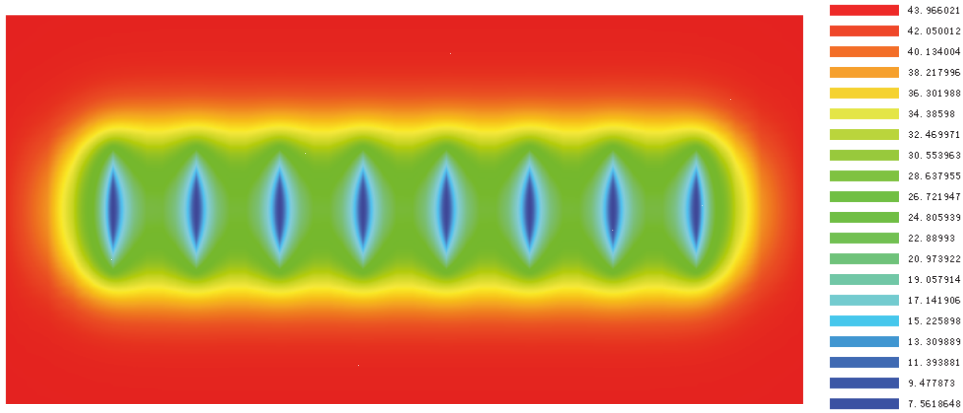

Figure 13: Contour of pressure at the 3024th hour.

6. Conclusions

Based on the analytical pressure distribution of a multifractured horizontal well in shale gas formation, the presented method is an analytical approach to calculate and determine the contribution of free and adsorbed gas to the production. The following conclusions can be drawn based on this study:

(1) Considering the pressure-sensitive, gas diffusing, and adsorption effects, the mathematical model of multifractured horizontal wells in fully closed rectangular

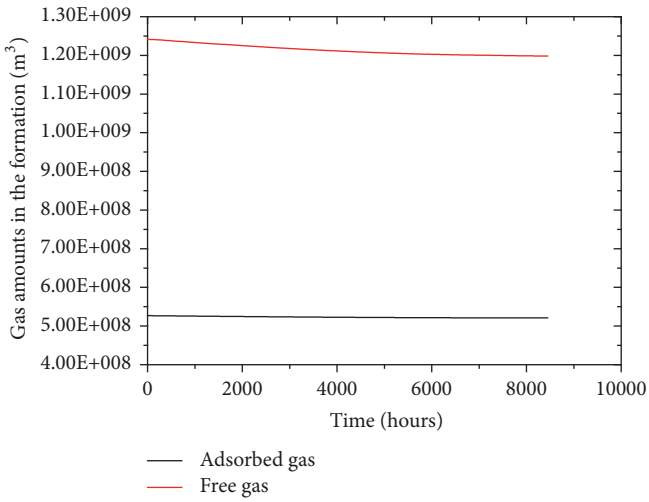

Figure 14: Amounts of adsorbed and free gas in the formation for case 2.

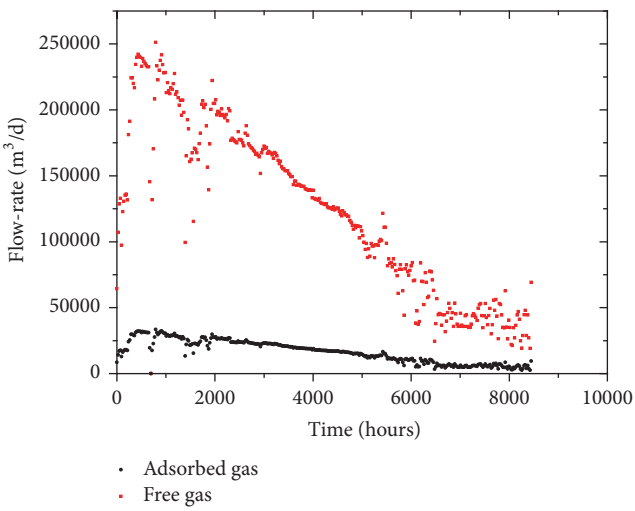

Figure 15: Flow-rates of adsorbed and free gas for case 2.

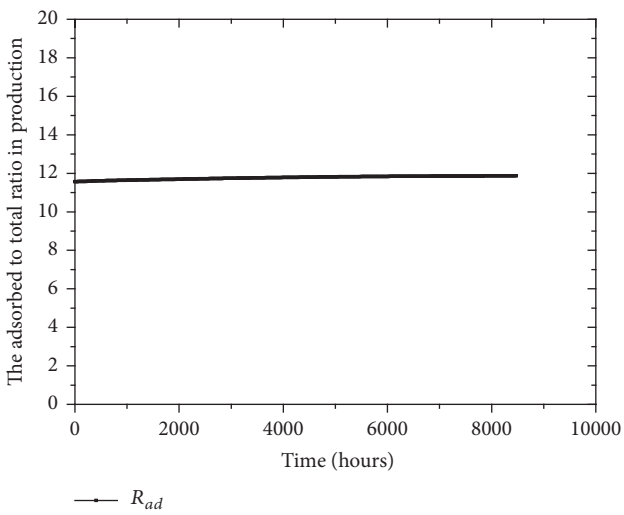

Figure 17: The adsorbed-to-total ratio R_{ad} in production.

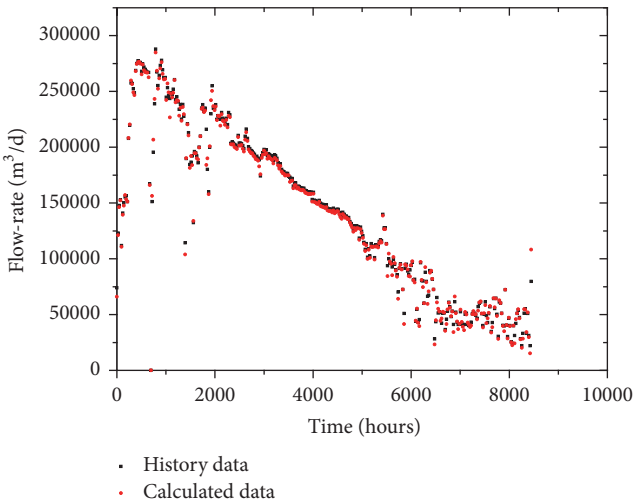

Figure 16: Comparison of calculated flow-rates and history data.

formations is established and the normalized pressure distribution in the formation is obtained analytically. Meanwhile, a numerical validation is conducted to verify the mathematical model.

(2) The amounts of adsorbed gas, matrix free gas, and fracture free gas in shale gas formations are expressed in integral form with the pressure distribution calculated. The fracture free gas can be ignored since it is much smaller as compared with matrix free gas and adsorbed gas.

(3) Two field example studies have been carried out. The calculated R_{ad} in shale gas production is about 10%. The average errors of history matching of gas production are acceptable (4% and 6%). The results indicate that the proposed method is reliable and efficient.

The related parametric study and the mentioned two-phase flow equation issue are underway. Besides, if the pressure distribution cannot be obtained analytically, numerical reservoir simulation is an alternative to obtain the pressure distribution, which is our future work.

Data Availability

The readers can access the data used in this paper by contacting the corresponding author.

Conflicts of Interest

The authors declare no conflicts of interest.

Acknowledgments

This work is supported by CAS Strategic Priority Research Program (Grant no. XDB10030402), CNPC-CAS Strategic Cooperation Research Program (Grant no. 2015A-4812), and National Natural Science Foundation of China (Grant no. 41672114).

References

[1] H. Yaritani and J. Matsushima, "Analysis of the energy balance of shale gas development," *Energies*, vol. 7, no. 4, pp. 2207–2227, 2014.

[2] EIA, "Shale gas production drives world natural gas production growth," in *Today in Energy*, 2016, http://www.eia.gov/todayinenergy/detail.php?id=27512.

[3] Y. Pang, M. Y. Soliman, H. Deng, and X. Xie, "Experimental and analytical investigation of adsorption effects on shale gas transport in organic nanopores," *Fuel*, vol. 199, pp. 272–288, 2017.

[4] F. P. Wang and R. M. Reed, "Pore networks and fluid flow in gas shales," in *Proceedings of the SPE Annual Technical Conference and Exhibition (ATCE '09)*, pp. 1550–1557, New Orleans, La, USA, October 2009.

[5] T. Zhang, G. S. Ellis, S. C. Ruppel, K. Milliken, and R. Yang, "Effect of organic-matter type and thermal maturity on methane adsorption in shale-gas systems," *Organic Geochemistry*, vol. 47, pp. 120–131, 2012.

[6] Y. Xia, Y. Jin, K. P. Chen, M. Chen, and D. Chen, "Simulation on gas transport in shale: The coupling of free and adsorbed gas," *Journal of Natural Gas Science and Engineering*, vol. 41, pp. 112–124, 2017.

[7] G. Chen, S. Lu, J. Zhang et al., "Keys to linking GCMC simulations and shale gas adsorption experiments," *Fuel*, vol. 199, pp. 14–21, 2017.

[8] S. A. Mengal and R. A. Wattenbarger, "Accounting for adsorbed gas in Shale gas reservoirs," in *Proceedings of the 17th Middle East Oil and Gas Show and Conference 2011, MEOS 2011*, pp. 643–657, Manama, Bahrain, September 2011.

[9] C. McGlade, J. Speirs, and S. Sorrell, "Methods of estimating shale gas resources - Comparison, evaluation and implications," *Energy*, vol. 59, pp. 116–125, 2013.

[10] G. R. King, "Material-balance techniques for coal-seam and Devonian shale gas reservoirs with limited water influx," *SPE Reservoir Engineering*, vol. 8, no. 1, pp. 67–72, 1993.

[11] M. P. Walsh, "Generalized approach to reservoir material balance calculations," *Journal of Canadian Petroleum Technology*, vol. 34, no. 1, pp. 55–63, 1995.

[12] R. J. Ambrose, R. C. Hartman, M. Diaz-Campos, I. Y. Akkutlu, and C. Sondergeld, "New pore-scale considerations for shale gas in place calculations," in *Proceedings of the SPE Unconventional Gas Conference*, SPE Paper 131772, Pittsburgh, Pa, USA, February 2010.

[13] D. Orozco and R. Aguilera, "A Material Balance Equation for Stress-Sensitive Shale Gas Reservoirs Considering the Contribution of Free, Adsorbed and Dissolved Gas," in *Proceedings of the SPE/CSUR Unconventional Resources Conference*, Calgary, Canada, 2015.

[14] Y. Liu, J. Zhang, and X. Tang, "Predicting the proportion of free and adsorbed gas by isotopic geochemical data: A case study from lower Permian shale in the southern North China basin (SNCB)," *International Journal of Coal Geology*, vol. 156, pp. 25–35, 2016.

[15] K. Liu, J. Sun, M. Gu, H. Liu, and X. Chen, "A new method for estimating the free-to-adsorbed ratio in shale gas reservoirs using acoustic amplitude attenuation and porosity," *Journal of Geophysics and Engineering*, vol. 14, no. 5, pp. 1042–1051, 2017.

[16] P. Zhang, L. Hu, J. N. Meegoda, and S. Gao, "Micro/Nano-pore Network Analysis of Gas Flow in Shale Matrix," *Scientific Reports*, vol. 5, 2015.

[17] Y. Jiang, Y. Luo, Y. Lu, C. Qin, and H. Liu, "Effects of supercritical CO2 treatment time, pressure, and temperature on microstructure of shale," *Energy*, vol. 97, pp. 173–181, 2016.

[18] I. Langmuir, "The adsorption of gases on plane surfaces of glass, mica and platinum," *Journal of the American Chemical Society*, vol. 40, no. 9, pp. 1361–1403, 1918.

[19] L. Ji, T. Zhang, K. L. Milliken, J. Qu, and X. Zhang, "Experimental investigation of main controls to methane adsorption in clay-rich rocks," *Applied Geochemistry*, vol. 27, no. 12, pp. 2533–2545, 2012.

[20] T. F. T. Rexer, M. J. Benham, A. C. Aplin, and K. M. Thomas, "Methane adsorption on shale under simulated geological temperature and pressure conditions," *Energy & Fuels*, vol. 27, no. 6, pp. 3099–3109, 2013.

[21] L. Zhou, Y. Zhou, M. Li, P. Chen, and Y. Wang, "Experimental and modeling study of the adsorption of supercritical methane on a high surface activated carbon," *Langmuir*, vol. 16, no. 14, pp. 5955–5959, 2000.

[22] R. O. Bello and R. A. Wattenbarger, "Multi-stage Hydraulically Fractured Horizontal Shale Gas Well Rate Transient Analysis," in *Proceedings of the North Africa Technical Conference and Exhibition*, Cairo, Egypt, 2010.

[23] Y.-L. Zhao, L.-H. Zhang, J.-Z. Zhao, J.-X. Luo, and B.-N. Zhang, ""Triple porosity" modeling of transient well test and rate decline analysis for multi-fractured horizontal well in shale gas reservoirs," *Journal of Petroleum Science and Engineering*, vol. 110, pp. 253–262, 2013.

[24] Z. Chen, X. Liao, X. Zhao, L. Zhu, and H. Liu, "Performance of multiple fractured horizontal wells with consideration of pressure drop within wellbore," *Journal of Petroleum Science and Engineering*, vol. 146, pp. 677–693, 2016.

[25] Z. Pan and L. D. Connell, "Reservoir simulation of free and adsorbed gas production from shale," *Journal of Natural Gas Science and Engineering*, vol. 22, pp. 359–370, 2015.

[26] J. E. Fitzgerald, Z. Pan, M. Sudibandriyo, R. L. Robinson Jr., K. A. M. Gasem, and S. Reeves, "Adsorption of methane, nitrogen,

carbon dioxide and their mixtures on wet Tiffany coal," *Fuel*, vol. 84, no. 18, pp. 2351–2363, 2005.

[27] H. Hu, F. Hao, X. Guo, F. Dai, Y. Lu, and Y. Ma, "Investigation of methane sorption of overmature Wufeng-Longmaxi shale in the Jiaoshiba area, Eastern Sichuan Basin, China," *Marine and Petroleum Geology*, vol. 91, pp. 251–261, 2018.

[28] P. Leclaire, O. Umnova, K. V. Horoshenkov, and L. Maillet, "Porosity measurement by comparison of air volumes," *Review of Scientific Instruments*, vol. 74, no. 3 I, pp. 1366–1370, 2003.

[29] L. Ghasemi-Mobarakeh, D. Semnani, and M. Morshed, "A novel method for porosity measurement of various surface layers of nanofibers mat using image analysis for tissue engineering applications," *Journal of Applied Polymer Science*, vol. 106, no. 4, pp. 2536–2542, 2007.

[30] K. Utpalendu, K. M. Douglas, D. Arkadiusz, B. F. Timothy, and P. Manika, "Total porosity measurement in gas shales by the water immersion porosimetry (WIP) method," *Fuel*, vol. 117, pp. 1115–1129, 2014.

[31] I. Palmer and J. Mansoori, "How Permeability Depends on Stress and Pore Pressure in Coalbeds: A New Model," *SPE Reservoir Engineering*, vol. 1, no. 6, pp. 539–543, 1998.

[32] X. Y. Kong, *Advanced Mechanics of Fluids in Porous Media*, University of Science and Technology of China Press, Hefei, China, 2nd edition, 2010.

[33] J.-J. Dong, J.-Y. Hsu, W.-J. Wu et al., "Stress-dependence of the permeability and porosity of sandstone and shale from TCDP Hole-A," *International Journal of Rock Mechanics and Mining Sciences*, vol. 47, no. 7, pp. 1141–1157, 2010.

[34] J. Liu, Z. Chen, D. Elsworth, H. Qu, and D. Chen, "Interactions of multiple processes during CBM extraction: A critical review," *International Journal of Coal Geology*, vol. 87, no. 3-4, pp. 175–189, 2011.

[35] H. Tang, Y. Di, Y. Zhang, and H. Li, "Impact of Stress-Dependent Matrix and Fracture Properties on Shale Gas Production," *Energies*, vol. 10, no. 7, p. 996, 2017.

[36] R. Raghavan and L. Y. Chin, "Productivity changes in reservoirs with stress-dependent permeability," *SPE Reservoir Evaluation and Engineering*, vol. 7, no. 4, pp. 308–315, 2004.

[37] H.-T. Wang, "Performance of multiple fractured horizontal wells in shale gas reservoirs with consideration of multiple mechanisms," *Journal of Hydrology*, vol. 510, pp. 299–312, 2014.

[38] A. F. van Everdingen, "The skin effect and its influence on the productive capacity of a well," *Journal of Petroleum Technology*, vol. 5, no. 6, pp. 171–176, 1953.

[39] J. C. Palacio and T. A. Blasingame, "Decline curve analysis using type curves—analysis of gas well production data," in *Proceedings of the Low Permeability Reservoirs Symposium*, Denver, CO, USA, 1993.

[40] A. C. Gringarten and H. J. Ramey Jr., "The use of source and green's function in solving unsteady-flow problem in reservoir ," *SPE Journal*, vol. 13, no. 5, pp. 285–296, 1973.

[41] R. N. Horne and K. O. Temeng, "Relative productivities and pressure transient modeling of horizontal wells with multiple fractures," in *Proceedings of the 9th Middle East Oil Show & Conference*, pp. 563–574, Sanabis, Bahrain, March 1995.

[42] L. G. Thompson and A. C. Reynolds, "Analysis of Variable-Rate Well-Test Pressure Data Using Duhamel's Principle," *SPE Formation Evaluation*, vol. 1, no. 5, pp. 453–469, 1986.

[43] H. Stehfest, "Numerical inversion of Laplace transforms," *Communications of the ACM*, vol. 13, no. 1, pp. 47–49, 1970.

[44] D. Li, L. Zhang, J. Y. Wang, D. Lu, and J. Du, "Effect of adsorption and permeability correction on transient pressures in organic rich gas reservoirs: Vertical and hydraulically fractured horizontal wells," *Journal of Natural Gas Science and Engineering*, vol. 31, pp. 214–225, 2016.